

A wideband generalization of the near-field region for extremely large phased-arrays

Nitish Deshpande, *Student Member, IEEE*, Miguel R. Castellanos, *Member, IEEE*, Saeed R. Khosravirad, *Member, IEEE*, Jinfeng Du, *Member, IEEE*, Harish Viswanathan, *Fellow, IEEE*, and Robert W. Heath Jr., *Fellow, IEEE*

Abstract

The narrowband and far-field assumption in conventional wireless system design leads to a mismatch with the optimal beamforming required for wideband and near-field systems. This discrepancy is exacerbated for larger apertures and bandwidths. To characterize the behavior of near-field and wideband systems, we derive the beamforming gain expression achieved by a frequency-flat phased array designed for plane-wave propagation. To determine the far-field to near-field boundary for a wideband system, we propose a frequency-selective distance metric. The proposed far-field threshold increases for frequencies away from the center frequency. The analysis results in a fundamental upper bound on the product of the array aperture and the system bandwidth. We present numerical results to illustrate how the gain threshold affects the maximum usable bandwidth for the n260 and n261 5G NR bands.

Index Terms

Near-field, wideband, phased-array, frequency-selective, beamforming gain.

I. INTRODUCTION

Distinguishing between the near-field and far-field is becoming increasingly relevant as modern wireless devices begin to operate in both propagation regions. The most common near-field distance, known as the Fraunhofer distance, is proportional to the square of the aperture and

Nitish Deshpande, Miguel R. Castellanos, and Robert W. Heath Jr. are with the Department of Electrical and Computer Engineering, North Carolina State University, Raleigh, NC 27606 USA (email: {nvdesHPa, mrcastel, rwheathjr}@ncsu.edu). Saeed R. Khosravirad, Jinfeng Du, and Harish Viswanathan are with Nokia Bell Laboratories, Murray Hill, NJ 07974, USA (email: {saeed.khosravirad, jinfeng.du, harish.viswanathan}@nokia-bell-labs.com). This project is funded by Nokia Bell Laboratories, Murray Hill, NJ 07974, USA.

inversely proportional to the wavelength [1]. To satisfy the data rate requirements of 5G and beyond, wireless systems have shifted to higher carrier frequencies and larger antenna arrays [2] [3]. For these modern arrays, the Fraunhofer distance becomes comparable to the typical cell radius. For example, the Fraunhofer array distance for a uniform linear array (ULA) with 128 antennas and half-wavelength inter-antenna spacing operating at 28 GHz is around 88 m. This is a good fraction of the cell radius of an urban microcellular and picocellular deployment [4]. In the near-field, the phase variation over the array aperture is non-linear in antenna index, which causes a phase mismatch when assuming far-field propagation with planar wavefronts [1] [5]. Inaccurate use of the far-field assumption can lead to beamforming gain losses that worsen as the array aperture increases [5].

Wideband systems with large arrays suffer from a phenomenon known as beam squint, i.e., the mismatch between the frequency-flat response of the phased-array and the frequency-selective response of the wideband channel. This reduces the beamforming gain for frequencies away from the center frequency. For wideband systems operating in the near-field, the two mismatches due to far-field and narrowband system design jointly affect the beamforming gain. Hence, it is crucial to characterize this combined effect for the performance analysis of large phased-array wideband systems.

Near-field and wideband effects have generally been considered separately in the literature. Various near-field metrics have been proposed in prior work [6], [7]. The definition of the Fraunhofer array distance is based on the phase variation of a monochromatic wave over the array length [1]. In [6], the proposed near-field metric used the amplitude variations as the criterion for determining the far-field to near-field transition distance. The metrics in [1], [6] did not consider the angle of incidence and have assumed broadside incidence only. The effective Rayleigh distance incorporates the incidence angle in the beamforming gain analysis [7]. One common shortcoming of these methods is that the beamforming gain analysis is restricted only for a single frequency and not for a band of frequencies. Although [8], [9] analyzed the beamforming gain for wideband systems and incorporated beam squint effect, they are based on the plane-wave approximation. To summarize, the existing work on the beamforming gain analysis either assumes a near-field and narrowband system [1], [6], [7] or a far-field and wideband system [8], [9].

In this letter, we analyze the beamforming gain of a multiple-input-single-output (MISO) communication system with ULA at transmitter for a general near-field and wideband channel

with a beamformer based on the far-field and narrowband assumption. For a large number of antennas, the beamforming gain can be approximated with a closed-form expression. The derived expression can be generalized to arbitrary carrier frequencies and array sizes. We propose the bandwidth-aware-near-field distance (BAND) to characterize the far-field to near-field transition in a wideband system. The BAND increases for frequencies away from the center frequency, which implies that wideband systems have a larger near-field region. Expressing the system parameters as a function of the beamforming gain uncovers a tradeoff between the aperture and bandwidth.

Notation: A bold lowercase letter \mathbf{a} denotes a vector, $(\cdot)^*$ denotes conjugate transpose, $|\cdot|$ indicates absolute value, $[\mathbf{a}]_n$ denotes the n th element of \mathbf{a} , $\mathcal{O}(\cdot)$ denotes the big Oh notation, $\mathcal{C}(\gamma) = \int_0^\gamma \cos(\frac{\pi}{2}t^2)dt$ and $\mathcal{S}(\gamma) = \int_0^\gamma \sin(\frac{\pi}{2}t^2)dt$ denote cosine and sine Fresnel functions, $\inf\{\cdot\}$ denotes the infimum.

II. SYSTEM MODEL

Let us assume a co-polarized single-user MISO communication system with an N antenna ULA at the transmitter and a single antenna at the receiver. All antennas are assumed to be isotropic. The transmitter is oriented along the x axis with inter-antenna spacing d . The x coordinate of the n th transmit antenna is defined as $d_n = \frac{2n-N+1}{2}d$ for $n = 0, 1, \dots, N-1$. The receiver is located at a distance r from the transmit array center, i.e., the origin, and at an angle θ with the y axis. The receiver location is $(r \sin(\theta), r \cos(\theta))$. The distance between the receive antenna and the n th transmit antenna is $r_n = \sqrt{r^2 - 2rd_n \sin(\theta) + d_n^2}$.

The channel is assumed to be a line-of-sight (LOS) path between the transmitter and receiver. The path can be characterized by the path loss and the path delay. The path loss between all transmit antennas and the receive antenna is assumed to be the same and denoted by $G(r)$. This assumption is valid for $r \sim \mathcal{O}(L)$ where $L = Nd$ is the array aperture [10]. Let f_c denote the center frequency of the passband signal and c denote the speed of light. The passband time-domain channel impulse response from the n th antenna is

$$[\mathbf{h}_p(t)]_n = \sqrt{G(r)}\delta\left(t - \frac{r_n}{c}\right). \quad (1)$$

The pseudo-complex baseband equivalent channel response after down-conversion is

$$[\mathbf{h}_b(t)]_n = \sqrt{G(r)}e^{-j2\pi\frac{r_n}{c}f_c}\delta\left(t - \frac{r_n}{c}\right). \quad (2)$$

The frequency-domain channel impulse response at baseband frequency f is

$$[\mathbf{h}(f)]_n = \sqrt{G(r)}e^{-j2\pi\frac{r_n}{c}(f_c+f)}. \quad (3)$$

The general channel response in (3) can be approximated under the narrowband and far-field assumptions. Under the narrowband assumption, the baseband frequency can be treated as small, i.e. $f \approx 0$. Taking the series expansion of the channel phase response around $f = 0$, we have $\exp(-j2\pi\frac{r_n}{c}(f_c+f)) = \exp(-j2\pi\frac{r_n}{c}(f_c + \mathcal{O}(f)))$. Under the far-field assumption, the distance r can be treated large, i.e., $r \rightarrow \infty$. Taking the series expansion of the channel phase response around $r \rightarrow \infty$, we have $\exp(-j2\pi\frac{r_n}{c}(f_c+f)) = \exp\left(-j2\pi\frac{(r-d_n\sin(\theta)+\mathcal{O}(\frac{1}{r}))}{c}(f_c+f)\right)$. Combining both of the expansions, we have, $\exp(-j2\pi\frac{r_n}{c}(f_c+f)) = \exp\left(-j2\pi\frac{(r-d_n\sin(\theta)+\mathcal{O}(\frac{1}{r}))}{c}(f_c+\mathcal{O}(f))\right)$ when the narrowband and far-field assumptions both hold. Using the subscripts nf, ff, wb, and nb to denote near-field, far-field, wideband, and narrowband assumptions, respectively, we summarize the four channel models, for the $N \times 1$ channel vectors, $\mathbf{h}_{\text{nf,wb}}(f)$, $\mathbf{h}_{\text{nf,nb}}$, $\mathbf{h}_{\text{ff,wb}}(f)$, and $\mathbf{h}_{\text{ff,nb}}$, in Table I.

TABLE I
SUMMARY OF THE CHANNEL MODELS

Channel response	Expression
$[\mathbf{h}_{\text{nf,wb}}(f)]_n$	$\sqrt{G(r)}e^{-j2\pi\frac{r_n}{c}(f_c+f)}$
$[\mathbf{h}_{\text{nf,nb}}]_n$	$\sqrt{G(r)}e^{-j2\pi\frac{r_n}{c}f_c}$
$[\mathbf{h}_{\text{ff,wb}}(f)]_n$	$\sqrt{G(r)}e^{-j2\pi\frac{(r-d_n\sin(\theta))}{c}(f_c+f)}$
$[\mathbf{h}_{\text{ff,nb}}]_n$	$\sqrt{G(r)}e^{-j2\pi\frac{(r-d_n\sin(\theta))}{c}f_c}$

The most general channel response is $\mathbf{h}_{\text{nf,wb}}(f)$. The optimal beamforming vector with unit norm constraint that maximizes the signal to noise ratio is $\mathbf{f}_{\text{nf,wb}}(f) = \frac{1}{\sqrt{NG(r)}}\mathbf{h}_{\text{nf,wb}}(f)$. Using a mismatched beamforming vector, i.e., $\mathbf{f} \neq \mathbf{f}_{\text{nf,wb}}(f)$ leads to beamforming gain loss. To characterize this mismatch, we define vectors $\mathbf{f}_{\text{nf,nb}}$, $\mathbf{f}_{\text{ff,wb}}(f)$, and $\mathbf{f}_{\text{ff,nb}}$ similarly.

Each of the four beamforming vectors allow different hardware implementations. The beamforming vectors $\mathbf{f}_{\text{ff,nb}}$ and $\mathbf{f}_{\text{nf,nb}}$ are frequency-flat and can be implemented using narrowband phase-shifters, whereas $\mathbf{f}_{\text{nf,wb}}(f)$ and $\mathbf{f}_{\text{ff,wb}}(f)$ are frequency-selective and can be implemented at higher cost as a fully-digital space-time precoder [11] or an analog true-time-delay architecture [12]. In this letter, we analyze the mismatch that occurs when using $\mathbf{f}_{\text{ff,nb}}$ for a near-field wideband

system. This analysis is crucial to characterize the scenarios where frequency-flat beamforming does not work well.

III. BEAMFORMING GAIN ANALYSIS

We analyze the performance loss due to $\mathbf{f}_{\text{ff,nb}}$ in terms of the normalized beamforming gain. The definitions of the normalized beamforming gains under different channel assumptions are summarized in Table II. The normalization is such that the maximum gain value is 0 dB.

TABLE II
DEFINITIONS OF NORMALIZED BEAMFORMING GAINS

Normalized beamforming gain	Expression
$\mu_{\text{nf,wb}}(f)$	$\frac{1}{\sqrt{G(r)N}} \mathbf{h}_{\text{nf,wb}}^*(f) \mathbf{f}_{\text{ff,nb}} $
$\mu_{\text{ff,wb}}(f)$ [9]	$\frac{1}{\sqrt{G(r)N}} \mathbf{h}_{\text{ff,wb}}^*(f) \mathbf{f}_{\text{ff,nb}} $
$\mu_{\text{nf,nb}}$ [5]	$\frac{1}{\sqrt{G(r)N}} \mathbf{h}_{\text{nf,nb}}^* \mathbf{f}_{\text{ff,nb}} $

The beamforming gain $\mu_{\text{ff,wb}}(f)$ only captures the wideband effect and $\mu_{\text{nf,nb}}$ only captures the near-field effect.

In Lemma 1, we express the inner product in $\mu_{\text{nf,wb}}(f)$ as a summation of the complex phases over N antennas. To express the phase in terms of dimensionless parameters, let the normalized distance be $\bar{r} = \frac{r}{\lambda_c}$, the normalized inter-antenna spacing be $\bar{d} = \frac{d}{\lambda_c}$, and the normalized frequency be $\bar{f} = \frac{f}{f_c}$. In the radiating near-field (Fresnel) region, i.e., $r_n > 0.5\sqrt{\frac{L^3}{\lambda_c}}$, the $\mathcal{O}(\frac{1}{r^2})$ term in the expansion of $r_n = r - d_n \sin(\theta) + \frac{d_n^2 \cos^2(\theta)}{2r} + \mathcal{O}(\frac{1}{r^2})$ can be ignored [1]. This assumption enables the decomposition of the phase for each antenna into two phase terms that individually capture the near-field and wideband phenomenon. At the n th antenna, we define the phase contribution due to the wideband assumption, $\phi_{\text{wb}} = -n\bar{d} \sin(\theta) \bar{f}$, and the phase contribution due to the near-field assumption, $\phi_{\text{nf}} = (\bar{f} + 1) \frac{\bar{d}^2}{2\bar{r}} \cos^2(\theta) (n - \frac{N-1}{2})^2$.

Lemma 1: In the Fresnel region, the near-field wideband beamforming gain can be approximated as $\mu_{\text{nf,wb}}^{\text{approx}}(\bar{f})$, where

$$\mu_{\text{nf,wb}}^{\text{approx}}(\bar{f}) = \left| \frac{1}{N} \sum_{n=0}^{N-1} e^{j2\pi(\phi_{\text{wb}} + \phi_{\text{nf}})} \right|. \quad (4)$$

Proof: The phase term in the inner product $\mathbf{h}_{\text{nf,wb}}^*(f)\mathbf{f}_{\text{ff,nb}}$ at the n th antenna is

$$\begin{aligned}
&= -\angle([\mathbf{h}_{\text{nf,wb}}(f)]_n) + \angle([\mathbf{f}_{\text{ff,nb}}]_n) \\
&\stackrel{(a)}{=} -\angle([\mathbf{h}_{\text{nf,wb}}(f)]_n) + \angle([\mathbf{h}_{\text{ff,nb}}]_n) \\
&\stackrel{(b)}{\approx} \frac{2\pi}{c} \left[\left(r - d_n \sin(\theta) + \frac{d_n^2 \cos^2(\theta)}{2r} \right) (f_c + f) \right. \\
&\quad \left. - (r - d_n \sin(\theta)) f_c \right], \tag{5}
\end{aligned}$$

where equality (a) follows from the definition of $\mathbf{f}_{\text{ff,nb}}$ and approximation (b) follows from Table I and expansion of r_n . By factoring out the terms which do not depend on the index n , and using the definition of \bar{f} , \bar{d} , and \bar{r} , we get (4). \square

Lemma 1 illustrates a few key insights. The expression for $\mu_{\text{nf,wb}}(f)$ depends only on the normalized parameters. Hence, this analysis is independent of the carrier frequency; the same beamforming gain can be obtained for different carrier frequencies provided that the normalized parameters remain fixed. The expression for the far-field wideband gain $\mu_{\text{ff,wb}}(f)$ in [9] can be obtained by setting $\phi_{\text{nf}} = 0$. The near-field narrowband gain $\mu_{\text{nf,nb}}$ in [5] can be obtained by setting $\phi_{\text{wb}} = 0$ and $\bar{f} = 0$. The phase ϕ_{wb} is linear and ϕ_{nf} is quadratic in the antenna index. Both ϕ_{wb} and ϕ_{nf} are dependent on \bar{f} . Hence, existing beamforming methods based on uniform spacing and narrowband assumption do not work well.

In Lemma 2, we further simplify (4) to get an expression in terms of Fresnel functions whose arguments depend on the system parameters. The purpose of this simplification is to establish a closed-form algebraic relationship between the system parameters and the beamforming gain threshold. We define the normalized array aperture as $\bar{L} = N\bar{d}$. Lemma 2 shows the relationship between the parameters, $\{\bar{f}, \bar{r}, \bar{L}, \theta\}$, and a 2D parameter space defined by γ_1 and γ_2 as

$$\gamma_1 = -\tan(\theta)\bar{f}\sqrt{\frac{2\bar{r}}{1+\bar{f}}}, \tag{6}$$

$$\gamma_2 = \bar{L}\cos(\theta)\sqrt{\frac{1+\bar{f}}{2\bar{r}}}. \tag{7}$$

The compression from four parameters to two new parameters γ_1 and γ_2 allows us to visualize the beamforming gain function. It also simplifies numerical simulations by varying γ_1 and γ_2 instead of varying four system parameters.

Lemma 2: The expression of $\mu_{\text{nf,wb}}^{\text{approx}}(\bar{f})$ in (4) can be further approximated for large N with fixed d as

$$\mathcal{G}(\gamma_1, \gamma_2) = \lim_{N \rightarrow \infty} \mu_{\text{nf,wb}}^{\text{approx}}(\bar{f}) = \left| \frac{\bar{\mathcal{C}}(\gamma_1, \gamma_2) + j\bar{\mathcal{S}}(\gamma_1, \gamma_2)}{2\gamma_2} \right|, \quad (8)$$

$\bar{\mathcal{C}}(\gamma_1, \gamma_2) \equiv \mathcal{C}(\gamma_1 + \gamma_2) - \mathcal{C}(\gamma_1 - \gamma_2)$ and $\bar{\mathcal{S}}(\gamma_1, \gamma_2) \equiv \mathcal{S}(\gamma_1 + \gamma_2) - \mathcal{S}(\gamma_1 - \gamma_2)$.

Proof: We rewrite (4) by defining $\Delta_m = \frac{1}{N}$ for $m = 0, \frac{1}{N}, \dots, \frac{N-1}{N}$, $a = \cos(\theta) \sqrt{\frac{(1+\bar{f})\bar{d}^2}{2\bar{r}}}$, and $b = \frac{1}{a} \left(\frac{(1+\bar{f})\bar{d}^2 \cos^2(\theta)(N-1)}{4\bar{r}} + \frac{\bar{d} \sin(\theta)\bar{f}}{2} \right)$ to get

$$\mu_{\text{nf,wb}}^{\text{approx}}(\bar{f}) = \left| \Delta_m \sum_{m=0}^{1-\frac{1}{N}} \exp(j2\pi(amN - b)^2) \right|. \quad (9)$$

As $N \rightarrow \infty$, we can express the summation in (9) as an integral using the Riemann integral method [5] as

$$\begin{aligned} \mu_{\text{nf,wb}}^{\text{approx}}(\bar{f}) &= \left| \int_0^1 \exp(j2\pi(aNt - b)^2) dt + \mathcal{O}\left(\frac{1}{N}\right) \right|, \\ &\stackrel{(a)}{=} \left| \frac{\int_{-2b}^{2aN-2b} \exp(j\frac{\pi}{2}(t')^2) dt'}{2aN} + \mathcal{O}\left(\frac{1}{N}\right) \right|, \end{aligned} \quad (10)$$

where (a) follows by letting $aNt - b = \frac{t'}{2}$. For large N , using $(N-1)\bar{d} \approx (N+1)\bar{d} \approx N\bar{d} = \bar{L}$, (6), (7), we get (8). \square

The expression derived in Lemma 2 simplifies to the narrowband case, i.e., $\bar{f} = 0$, by substituting $\gamma_1 = 0$ in (8). Hence, the near-field narrowband gain for large N is defined as $\mathcal{G}^{\text{nb}}(\gamma_2) = \lim_{N \rightarrow \infty} \mu_{\text{nf,nb}} = \left| \frac{\mathcal{C}(\gamma_2) + j\mathcal{S}(\gamma_2)}{\gamma_2} \right|$, which is the same near-field gain expression derived in [5] and [7]. We have generalized $\mathcal{G}^{\text{nb}}(\gamma_2)$ [5], [7] by incorporating the bandwidth effect through the parameter γ_1 .

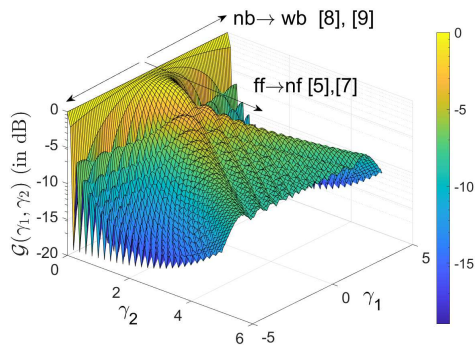


Fig. 1. 3D plot of $\mathcal{G}(\gamma_1, \gamma_2)$ vs γ_1 and γ_2 in dB scale. Increase in $|\gamma_1|$ corresponds to transition from narrowband to wideband; increase in γ_2 corresponds to transition from far-field to near-field.

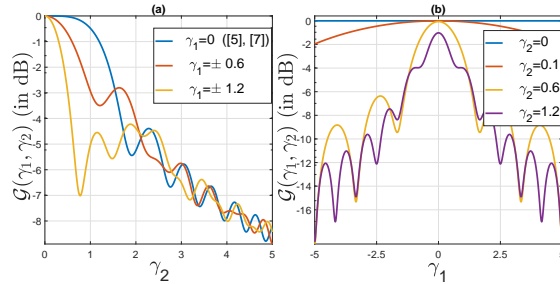


Fig. 2. 2D cross-sections of $\mathcal{G}(\gamma_1, \gamma_2)$ in dB scale. (a) $\mathcal{G}(\gamma_1, \gamma_2)$ vs γ_2 for a fixed $|\gamma_1|$; (b) $\mathcal{G}(\gamma_1, \gamma_2)$ vs γ_1 for a fixed γ_2 .

In Fig. 1, we study the variation of $\mathcal{G}(\gamma_1, \gamma_2)$ with γ_1 and γ_2 to understand the beamforming gain dependence on the system parameters. There is a drastic reduction in $\mathcal{G}(\gamma_1, \gamma_2)$ with increase in $|\gamma_1|$ and γ_2 . Note that the function $\mathcal{G}(\gamma_1, \gamma_2)$ is an even function with respect to γ_1 . This reflects the fact that the beamforming gain is symmetric with respect to θ .

The 2D cross-sections of the beamforming gain are shown in Fig. 2. In Fig. 2 (a), we keep γ_1 fixed and plot $\mathcal{G}(\gamma_1, \gamma_2)$ as a function of γ_2 . Assuming a non-zero angle θ , the 2D plot corresponding to $\gamma_1 = 0$, shown in blue, represents the narrowband case which is same as the plot shown in prior work on near-field propagation [5], [7]. The parameter γ_2 captures the transition from far-field to near-field in [7]. The effective Rayleigh distance, $d_{\text{ERD}}(\theta) = 0.367 \cos^2(\theta)(2\bar{L}^2\lambda_c)$, is defined using (7) with $\bar{f} = 0$, as the distance below which the value of the beamforming gain $\mathcal{G}^{\text{nb}}(\gamma_2)$ falls under the threshold 0.95 in linear scale [7]. We observe that for the wideband case, i.e., $\bar{f} \neq 0$, the value of $\mathcal{G}(\gamma_1, \gamma_2)$ drops sharply with γ_2 as $|\gamma_1|$ increases. In Fig. 2 (b), γ_2 is fixed and we plot $\mathcal{G}(\gamma_1, \gamma_2)$ as a function of γ_1 . For small values of γ_2 , the peak value is close to 0 dB. However, for larger values of γ_2 , the peak value drops and the main lobe shrinks. These results suggest that the joint effect of γ_1 and γ_2 is more severe than their individual effect.

The 2D cross-sections of the 3D plot in Fig. 1 resemble the plots from existing works [7]–[9] which study the wideband and near-field phenomena separately. The 3D plot jointly models the wideband and near-field effects. We analyze the connections of $\{\gamma_1, \gamma_2\}$ with $\{\bar{f}, \bar{r}, \bar{L}, \theta\}$ in Section IV.

IV. INVERSE MAPPING OF BEAMFORMING GAIN TO SYSTEM PARAMETERS SPACE

Most of the existing studies [1], [6]–[9] analyze the beamforming gain as a function of the different system parameters. From a system design perspective, however, it is essential to understand the inverse relationship for each system parameter as a function of the beamforming gain and other system parameters. We identify a fundamental tradeoff between the aperture and bandwidth in Section IV-A. We also establish a frequency-selective near-field boundary distance in Section IV-B.

A. Aperture-bandwidth product

In Section III, we introduced the beamforming gain dependence on \bar{f} through γ_1 and γ_2 . From (6) and (7), the normalized frequency \bar{f} can be expressed as

$$\bar{f} = -\frac{\gamma_1\gamma_2}{\bar{L}\sin(\theta)}. \quad (11)$$

We also define the fractional bandwidth as $f_B = |2\bar{f}|$. Hence, from (11), we have the relation

$$|f_B\bar{L}\sin(\theta)| = |2\gamma_1\gamma_2|. \quad (12)$$

To understand the maximum limit up to which the aperture and/or bandwidth can be scaled up while maintaining the narrowband and far-field assumption, we are interested in the maximum limit of the right hand side of (12) which can be found numerically for a given value of $\mathcal{G}(\gamma_1, \gamma_2)$.

We show the 2D contour plot version of Fig. 1 in Fig. 3. The contour plot is defined as the locus of the points in the (γ_1, γ_2) space which achieve a fixed value of the beamforming gain $\mathcal{G}(\gamma_1, \gamma_2)$. The pair of hyperbola marked in red, $|\gamma_1\gamma_2| = 0.5044$, corresponds to $\mathcal{G}(\gamma_1, \gamma_2) = -2$ dB. The pair of hyperbola marked in blue, $|\gamma_1\gamma_2| = 0.3654$, corresponds to $\mathcal{G}(\gamma_1, \gamma_2) = -1$ dB. Hence, from (12) and Fig. 3, we conclude that to maintain a beamforming gain, $\mathcal{G}(\gamma_1, \gamma_2) \in [-2, -1]$ dB, $|f_B\bar{L}\sin(\theta)|$ must approximately lie in the range $[0.73, 1]$. The upper limit on $|f_B\bar{L}\sin(\theta)|$ decreases as the threshold increases. From a system design perspective, the worst case angle of incidence θ_{worst} can be chosen based on the sector division. Hence, we get the worst case upper bound on $f_B\bar{L}$ as $f_B\bar{L} \leq \left| \frac{2\gamma_1\gamma_2}{\sin(\theta_{\text{worst}})} \right|$. In terms of un-normalized parameters, this simplifies to an important fundamental constraint on the product of the bandwidth, B , and the array aperture, L , as

$$BL \leq \left| \frac{2c\gamma_1\gamma_2}{\sin(\theta_{\text{worst}})} \right|. \quad (13)$$

The relationship in (13) plays an important role in determining the limits on the system design parameters for a particular beamforming gain. We define the maximum usable bandwidth, for a fixed aperture L , that achieves beamforming gain τ , for the worst case incidence angle, as $B_{\max} = \left\lfloor \frac{2c[\gamma_1\gamma_2]_{\max}}{L \sin(\theta_{\text{worst}})} \right\rfloor$, where $[\gamma_1\gamma_2]_{\max}$ is computed numerically for a given τ . If the system bandwidth exceeds B_{\max} , the beamforming gain drops below the required threshold.

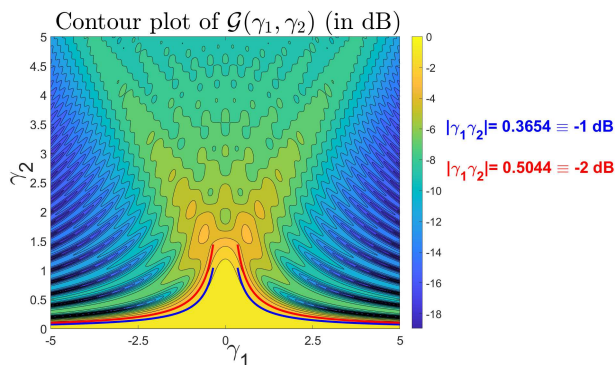


Fig. 3. Contour plot of $\mathcal{G}(\gamma_1, \gamma_2)$ in dB scale. The hyperbolas determine upper bound on the aperture-bandwidth product for a fixed beamforming gain.

Remark 1: We observe that $f_B \bar{L}$ can also be written as the ratio of the maximum propagation delay difference across the array to the symbol duration T_s , i.e., $f_B \bar{L} = \frac{Nd/c}{T_s}$. In [13], the upper bound on $f_B \bar{L}$ was loosely specified using $Nd/c \ll T_s$. The bound proposed in (13) is more precise.

B. Bandwidth-aware-near-field distance (BAND)

We use the relationship in (7) to derive a frequency-dependent near-field distance. The normalized distance, \bar{r} , can be written as a function of \bar{f} , γ_2 , \bar{L} , and θ as

$$\bar{r}(\bar{f}, \gamma_2, \bar{L}, \theta) = \frac{\bar{L}^2 \cos^2(\theta)(1 + \bar{f})}{2\gamma_2^2}. \quad (14)$$

The BAND is the smallest distance beyond which the beamforming gain is always above a certain threshold τ . By expressing γ_1 using $\{\bar{f}, \gamma_2, \bar{L}, \theta\}$, the BAND is defined as

$$\text{BAND}(f, f_c, \tau, L, \theta) = \inf \left\{ \lambda_c \bar{r}' : \mathcal{G} \left(\frac{-\bar{f} \bar{L} \sin(\theta)}{\gamma_2}, \gamma_2 \right) \geq \tau, \right. \\ \left. \forall \bar{r}'(\bar{f}, \gamma_2, \bar{L}, \theta) \geq \bar{r}' \right\}. \quad (15)$$

The BAND is computed using (14) from $\left(\frac{-\bar{f}L \sin(\theta)}{\gamma_2}, \gamma_2\right)$, which is obtained numerically for a τ from Fig. 3.

The BAND is related to the distances defined only for the narrowband case, i.e., $\bar{f} = 0$, as follows:

- Effective Rayleigh distance [7]: $d_{\text{ERD}}(\theta) = \text{BAND}(0, f_c, -0.2\text{dB}, L, \theta)$.
- Fraunhofer array distance [1]: $d_{\text{FA}} = 2\bar{L}^2\lambda_c = \text{BAND}(0, f_c, -0.04\text{dB}, L, 0^\circ)$.

The BAND is a wideband generalization of the near-field distances proposed in [1] and [7]. The BAND also determines the favorable regime for a transceiver hardware operating at any general frequency offset from f_c .

V. NUMERICAL RESULTS

The analysis presented in Section III and Section IV holds for any carrier frequency. In this section, we provide illustrations for some specific carrier frequencies currently used in the 5G standards [14].

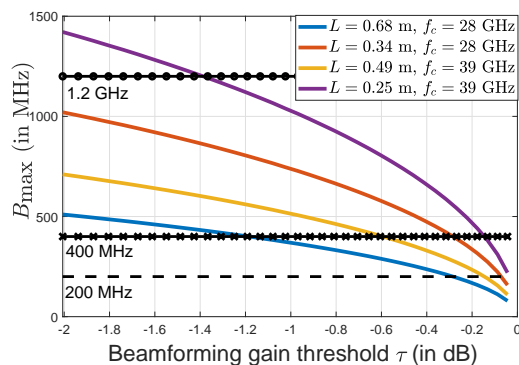


Fig. 4. B_{\max} as a function of the beamforming gain threshold for $\{L, f_c\} \equiv (0.68 \text{ m}, 28 \text{ GHz}), (0.34 \text{ m}, 28 \text{ GHz}), (0.49 \text{ m}, 39 \text{ GHz}), (0.25 \text{ m}, 39 \text{ GHz})$. Tradeoff between gain threshold and maximum usable bandwidth is illustrated.

In Fig. 4, B_{\max} is plotted as a function of the beamforming gain threshold for $\theta_{\text{worst}} = 60^\circ$. For n261 band in 5G NR [14], $f_c = 28 \text{ GHz}$. For n260 band in 5G NR [14], $f_c = 39 \text{ GHz}$. For each band, we plot B_{\max} for $N = \{64, 128\}$. We also mark the bandwidths of 200 MHz, 400 MHz, and 1.2 GHz.

Fig. 4 offers two important insights. For a given $\{L, f_c\}$ pair, we can determine the maximum possible beamforming gain for the 5G NR bandwidths. Conversely, we can also determine B_{\max}

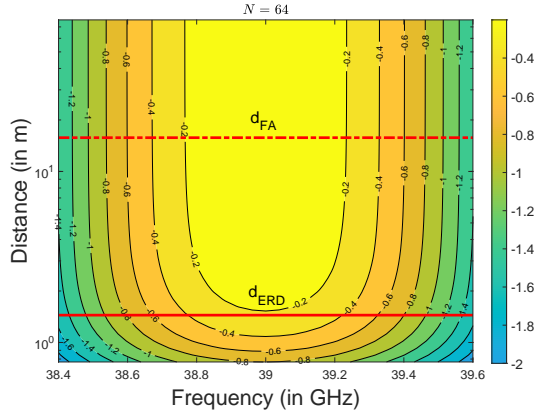


Fig. 5. Contour plot of beamforming gain (in dB) as a function of distance (in m) and frequency (in GHz) for $f_c = 39$ GHz and $N = 64$. The BAND attains a global minima at f_c .

for a fixed value of beamforming gain. As expected from (13), for a fixed f_c , B_{\max} doubles as L gets halved to maintain the same beamforming gain.

In Fig. 5, we show the contour plot in Fig. 3 with a change of variables from (γ_1, γ_2) to the (r, f) space using (11) and (14) for $\bar{d} = 0.5$, $\theta = 60^\circ$, $f_c = 39$ GHz and for $N = 64$. Each contour denotes the BAND for a given gain threshold. For operating distances greater than the BAND, the beamforming gain will always remain above the threshold. The plot shows that the distance increases for frequencies away from the center frequency. This distance diverges beyond a certain value of frequency $|f|$, which illustrates the concept of the maximum usable bandwidth derived in (13). In Fig. 5, we also plot d_{ERD} and d_{FA} which are same for all frequencies in the band. The distance d_{FA} is inaccurate because it does not incorporate the angle dependence and frequency-selectivity. The distance d_{ERD} is consistent with the BAND value for $\tau = -0.2$ dB only at the center frequency 39 GHz because d_{ERD} is derived using a narrowband model. The distance d_{ERD} underestimates the near-field distance for frequencies away from f_c .

VI. CONCLUSION

In this letter, we proposed a new definition of the beamforming gain metric which incorporates both wideband and near-field propagation effects. For a MISO system with a ULA at the transmitter, we provided a simple closed-form expression for the beamforming gain in terms of standard Fresnel functions with two parameters that model the near-field and wideband effects. A key observation is that the beamforming gain depends only on the normalized frequency and normalized distances, which enables the validity of the insights for any carrier frequency. The

proposed upper bound on the aperture-bandwidth product is beneficial for characterizing the performance of the existing frequency-flat beamforming when scaling up in carrier frequency, bandwidth, and array aperture. We showed that the BAND corresponding to a particular threshold attains minima at f_c and increases for frequencies away from f_c . The model and analysis presented in this work is especially relevant for short distance transmission where the near-field effect is more relevant, with potentially small impact from angular spread. We encourage future studies to address the impact of angular spread on beamforming gain. Other future directions of work include extending the BAND definition to planar arrays, the MIMO LOS channel, and incorporating the mutual coupling effect for dense arrays.

REFERENCES

- [1] K. T. Selvan and R. Janaswamy, "Fraunhofer and Fresnel distances: Unified derivation for aperture antennas." *IEEE Antennas Wireless Propag. Mag.*, vol. 59, no. 4, pp. 12–15, Aug. 2017.
- [2] S. Tripathi, N. V. Sabu, A. K. Gupta, and H. S. Dhillon, "Millimeter-wave and terahertz spectrum for 6G wireless," in *6G Mobile Wireless Networks*. Cham: Springer International Publishing, 2021, pp. 83–121.
- [3] R. W. Heath Jr., N. Gonzalez-Prelcic, S. Rangan, W. Roh, and A. M. Sayeed, "An overview of signal processing techniques for millimeter wave MIMO systems," *IEEE J. Sel. Topics Signal Process.*, vol. 10, no. 3, pp. 436–453, Apr. 2016.
- [4] S. Rangan, T. S. Rappaport, and E. Erkip, "Millimeter-wave cellular wireless networks: Potentials and challenges," *Proc. IEEE*, vol. 102, no. 3, pp. 366–385, 2014.
- [5] M. Cui and L. Dai, "Channel estimation for extremely large-scale MIMO: far-field or near-field?" *IEEE Trans. Commun.*, pp. 1–1, 2022.
- [6] E. Björnson and L. Sanguinetti, "Power scaling laws and near-field behaviors of massive MIMO and intelligent reflecting surfaces," *IEEE Open J. Commun. Soc.*, vol. 1, pp. 1306–1324, 2020.
- [7] M. Cui, L. Dai, R. Schober, and L. Hanzo, "Near-field wideband beamforming for extremely large antenna arrays," *arXiv:2109.10054*.
- [8] M. Cai, K. Gao, D. Nie, B. Hochwald, J. N. Laneman, H. Huang, and K. Liu, "Effect of wideband beam squint on codebook design in phased-array wireless systems," in *Proc. IEEE Globecom*, 2016, pp. 1–6.
- [9] F. Gao, B. Wang, C. Xing, J. An, and G. Y. Li, "Wideband beamforming for hybrid massive MIMO terahertz communications," *IEEE J. Sel. Areas Commun.*, vol. 39, no. 6, pp. 1725–1740, Jun. 2021.
- [10] H. Lu and Y. Zeng, "Communicating with extremely large-scale array/surface: Unified modelling and performance analysis," *IEEE Trans. Wireless Commun.*, vol. 21, June 2022.
- [11] R. C. Daniels and R. W. Heath, "MISO precoding for temporal and spatial focusing," in *Proc. Int. Symp. Wirel. Commun. Syst.*, vol. 6, Aalborg, Denmark, 2005, pp. 18–22.
- [12] R. Rotman, M. Tur, and L. Yaron, "True time delay in phased arrays," *Proc. IEEE*, vol. 104, no. 3, pp. 504–518, Mar. 2016.
- [13] S. Jang, R. Lu, J. Jeong, and M. P. Flynn, "A 1-GHz 16-element four-beam true-time-delay digital beamformer," *IEEE J. Solid-State Circuits*, vol. 54, no. 5, pp. 1304–1314, May 2019.
- [14] F. Launay, *5G-NR Radio Interface – Operations on the Frequency Bands*, 2021, pp. 141–160.

This figure "preview-micro.jpg" is available in "jpg" format from:

<http://arxiv.org/ps/2206.14323v1>

This figure "preview-web.jpg" is available in "jpg" format from:

<http://arxiv.org/ps/2206.14323v1>

This figure "preview.jpg" is available in "jpg" format from:

<http://arxiv.org/ps/2206.14323v1>